Journal Pre-proofs

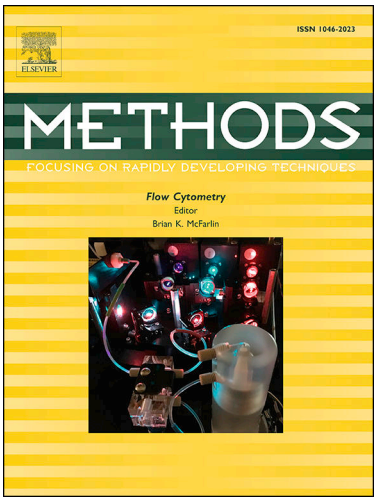

Analysis of non-canonical three- and four-way DNA junctions

Bríonna McGorman, Simon Poole, Miguel Vázquez López, Andrew Kellett

PII: S1046-2023(23)00145-7
DOI: https://doi.org/10.1016/j.ymeth.2023.09.002
Reference: YMETH 5389

To appear in: *Methods*

Received Date: 4 July 2023
Revised Date: 1 September 2023
Accepted Date: 5 September 2023

Please cite this article as: B. McGorman, S. Poole, M.V. López, A. Kellett, Analysis of non-canonical three- and four-way DNA junctions, *Methods* (2023), doi: https://doi.org/10.1016/j.ymeth.2023.09.002

Analysis of non-canonical three- and four-way DNA junctions

Bríonna McGorman,[†a] Simon Poole,[†a] Miguel Vázquez López,[b] and Andrew Kellett*[a]

[a] SSPC, the Science Foundation Ireland Research Centre for Pharmaceuticals, School of Chemical Sciences, Dublin City University Glasnevin, Dublin 9, Ireland.

[b] Centro Singular de Investigación en Química Biolóxica e Materiais Moleculares (CiQUS) and Departamento de Química Inorgánica. Universidade de Santiago de Compostela. Rúa Jenaro de la Fuente s/n, 15782 Santiago de Compostela, Spain.

[†] Authors contributed equally to this work.

* Corresponding author. E-mail address: andrew.kellett@dcu.ie.

Highlights

- We report a multiplex fluorescence polyacrylamide gel electrophoresis (PAGE) method for visualising and characterising three- and four-way DNA junctions.
- We also report how microscale thermophoresis can be employed in tandem with PAGE to quantify the formation of three- and four-way DNA junctions.
- These methods are suitable to probe the junction binding properties of small molecules and molecular helicates and can be used to compare their relative binding interactions in comparison to duplex DNA.

Abstract

The development of compounds that can selectively bind with non-canonical DNA structures has expanded in recent years. Junction DNA, including three-way junctions (3WJs) and four-way Holliday junctions (HJs), offer an intriguing target for developmental therapeutics as both 3WJs and HJs are involved in DNA replication and repair processes. However, there are a limited number of assays available for the analysis of junction DNA binding. Here, we describe the design and execution of multiplex fluorescent polyacrylamide gel electrophoresis (PAGE) and microscale thermophoresis (MST) assays that enable evaluation of junction-binding compounds. Two well characterised junction-binding compounds—a C6 linked bis-acridine ligand and an iron(II)-bound peptide helicate, which recognise HJs and 3WJs, respectively—were employed as probes for both MST and PAGE experiments. The multiplex PAGE assay expands beyond previously reported fluorescent PAGE as it combines four individual fluorophores that can be combined to visualise single-strands, pseudo-duplexes, and junction DNA present during 3WJ and HJ formation. The use of MST to identify the binding affinity of junction binding agents is, to our knowledge, first reported example of this technique. The combined use of PAGE and MST provides complementary results for the visualisation of 3WJ and HJ formation and the direct binding affinity (K_d and EC_{50}) of these agents. These assays can be used to aid the discovery and design of new therapeutics targeting non-canonical nucleic acid structures.

Graphical Abstract

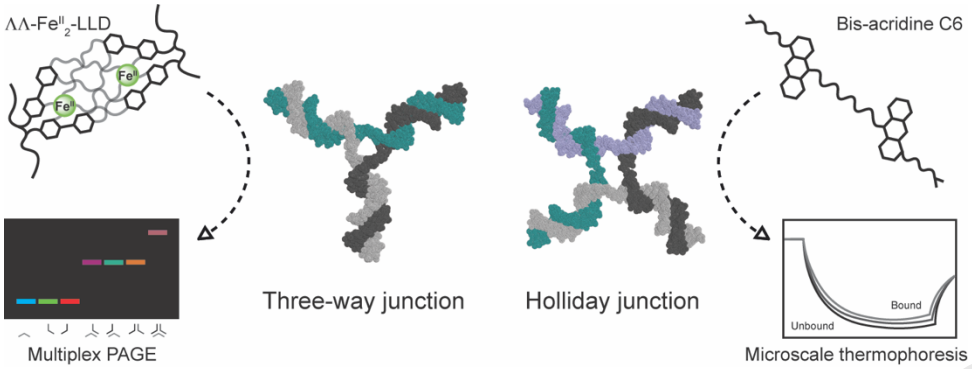

Keywords

Three-way junction; Holliday junction; Multiplex PAGE; Microscale thermophoresis; Peptide helicate; Bis-acridine.

Abbreviations

3WJ = Three-way junction

HJ = Holliday junction

G4 = G-quadruplex

BA-C6 = Bis-acridine with C6 linker

MST = Microscale thermophoresis

PAGE = Polyacrylamide gel electrophoresis

TBE = Tris-borate-EDTA

dsDNA = double-stranded DNA

AF350 = AlexaFluor™ 350

FAM = Fluorescein

ROX = Carboxy-X-rhodamine

Cy5 = Cyanine-5

Ex. = Excitation

Em. = Emission

1. Introduction

Since the structure of DNA was first eluded in 1953 by Watson and Crick,[1] Franklin[2] and Wilkins,[3] our knowledge of the structure and function of DNA has greatly expanded. DNA is a major target for many small molecules and targeted therapies. Many of these therapeutics bind with double-stranded DNA (dsDNA) but lack specific genetic targeting. Consequently, there is significant interest in developing compounds that bind sequence specifically or with higher order nucleic acid structures. In particular, non-canonical DNA structures, such as three-way junctions (3WJs),[4] Holliday junctions (HJs),[5] G-quadruplexes (G4s)[6] and I-motifis,[7] have become a focus within the field of targeted therapeutics. G4s and I-motifs are typically found within telomeric DNA and have been the focus of structural therapies in recent years.[8-10] However, much less work has been reported on chemical compounds that bind with junction DNA. DNA junctions, including 3WJs and HJs, are unique branched structures that consist of several double stranded DNA sequences converging at a single point, which is known as the branch point[11,12] (Figure 1). These structures play important roles as intermediates during genetic rearrangement processes, including DNA replication[13] and homologous recombination,[14, 15] which makes them important emerging therapeutic targets.

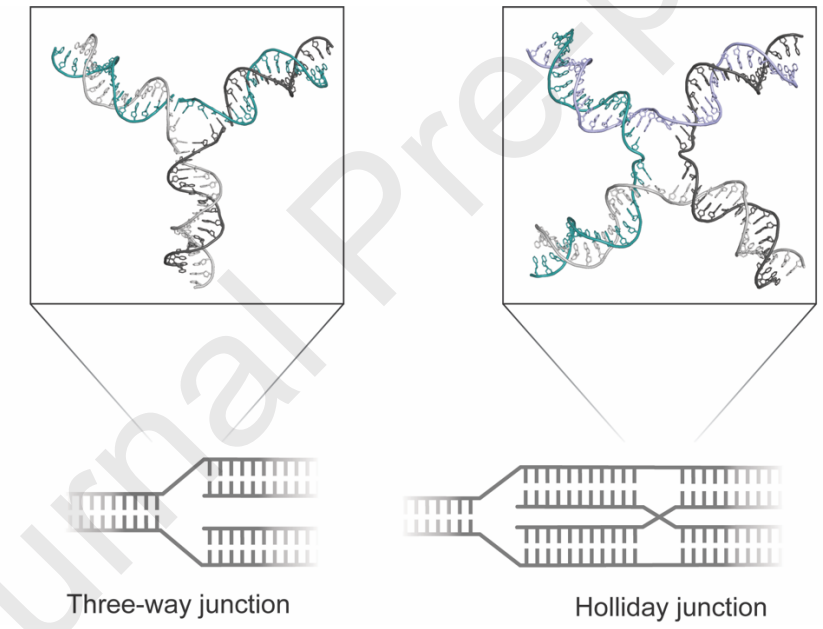

Figure 1. Crystal structure of 3WJ and HJ DNA. 3WJ and HJ were adapted from PDB: 1F44 and 3CRX, respectively.

3WJs are the simplest branched nucleic acid structure and consist of three strands of DNA that are partially complementary to each other. They are formed transiently during assembly of the replication fork during DNA replication and are therefore of interest as a biological target. Various compounds have been synthesised to selectively bind with, or stabilise 3WJs, including peptide-based supramolecular helicates[11, 16-19], three-fold symmetric triptycene derivatives,[19] and small molecules.[20] For this study, we selected a 3WJ DNA binding peptide helicate ($\Lambda\Lambda$-Fe^{II}_2LLD)[17] as the molecule of choice for our assay development.

HJs are sequence dependent 4-way junctions that play essential roles in regulating DNA functionality by mediating recombination and repair processes. HJs have two structural conformations, open-X and stacked-X, the latter of which has two isoforms[21] (Figure 2). The conformation adopted by the HJ is dependent on several variables including pH, salt concentration, and presence of recognition elements. Early work probing the HJ sought to understand the cleavage profile of metallodrugs with the branched structure, and subsequent analysis with dyes and porphyrins. Several recent HJ binding compounds have been reported, including peptides,[22] psoralen derivatives,[23] ATR inhibitors,[24] organometallic pillarplexes,[25] and bis-acridine compounds.[26] In particular, a bis-acridine compound with a C6 linker (BA-C6) has been shown to efficiently bind with and induce HJ formation through molecular assays[27, 28] and crystallography studies.[26] However, the development of new *in vitro* molecular assays that take advantage of recent advancements in fluorescence and immobilisation-free binding methods have yet to be reported.

Herein, we report new multiplex PAGE and microscale thermophoresis methods used to characterise the recognition of 3WJ and HJ DNA.

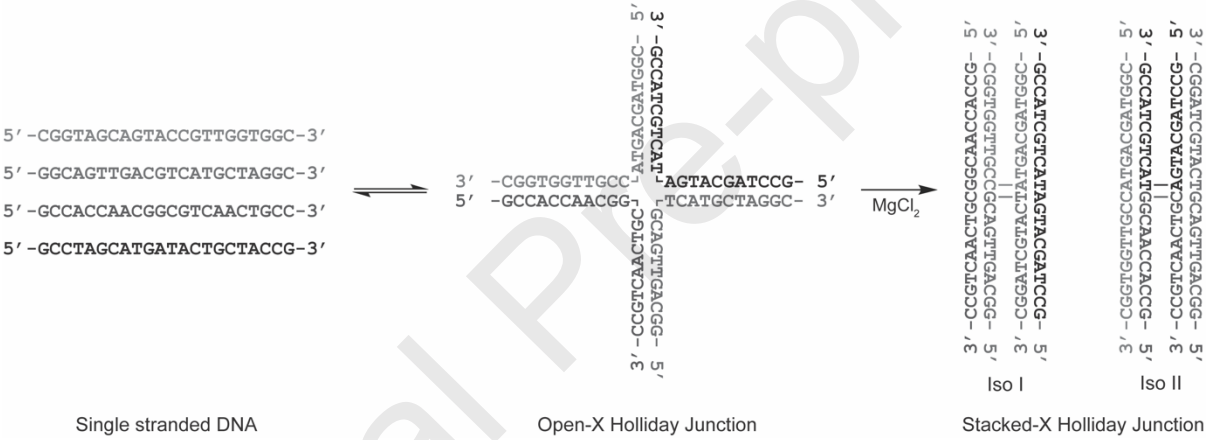

Figure 2. Single strands of HJ DNA and the open-X HJ are in equilibrium in water, but the addition of $MgCl_2$ enables the HJ to adopt the stacked-X forms.

2. Materials and Methods

2.1 Synthesis of 3WJ and HJ binding compounds

2.1.1 Synthesis of LLD helicate

The LLD peptide ligand was synthesised using Fmoc solid-phase peptide synthesis protocols as previously described[17] and Fe(II) was allowed to coordinate it (2:1, Fe(II):LLD) giving rise to the corresponding dinuclear Fe(II) peptide helicate.

2.1.2 Synthesis of Bis-acridine

BA-C6 was synthesised using a method previously described[29,30] and purified using column chromatography. The tetrahydrochloride salt of the compound was obtained by solubilising the BA-C6 freebase in a 1:1 chloroform:methanol mixture and titrating HCl into the stirring mixture, followed by vacuum reduction. The subsequent yellow powder of the tetrahydrochloride salt was obtained by redissolving the compound in methanol followed by precipitation with ethyl acetate and isolated by vacuum filtration.

2.2 Fluorescent oligonucleotide sequences

Fluorescently labelled oligomers were required to visualise non-canonical structures that arise when partially complementary 3WJ and HJ strands hybridise upon incubation at 37 ºC. To visualise individual strands fluorophores without overlapping emissions were selected, such that multiplex gel electrophoresis could be performed. Fluorescence SpectraViewer (ThermoFisher Scientific) was employed to identify the excitation and emission profiles of suitable fluorophores (Figure 3). Fluorescein (FAM), carboxy-X-rhodamine (ROX) and cyanine-5 (Cy5) were selected as appropriate labels for the 3WJ strands (`Y1-FAM`, `Y2-ROX` and `Y3-Cy5`), while Alexa Fluor™ 350 (AF350), FAM, ROX and Cy5 were selected for the HJ (`B-Cy5`, `H-AF350`, `R-ROX` and `X-FAM`). HJ strands (`B`, `H`, `R` and `X`) are named according to literature nomenclature, which originated from unique restriction sites on each arm proximate to the junction's core within an 80 bp HJ sequence developed by Duckett *et al*.,[31] which can be shortened by specific restriction enzymes (BamHI, HindIII, EcoRI and XbaI). A fluorescently labelled *off*-target DNA duplex was designed in parallel to visualise *off*-target effects of 3WJ and HJ binding compounds. A spacer sequence of four thymine bases, shown in blue, was included on all strands to ensure the fluorophore did not interfere with ligand binding. Fluorophore labelled sequences were purchased from Integrated DNA Technologies, re-dissolved to 100 μM according to manufacturer guidelines, and their concentration was confirmed by measuring absorbance at 260 nm (Nanodrop 1000, Themo Fisher Scientific).

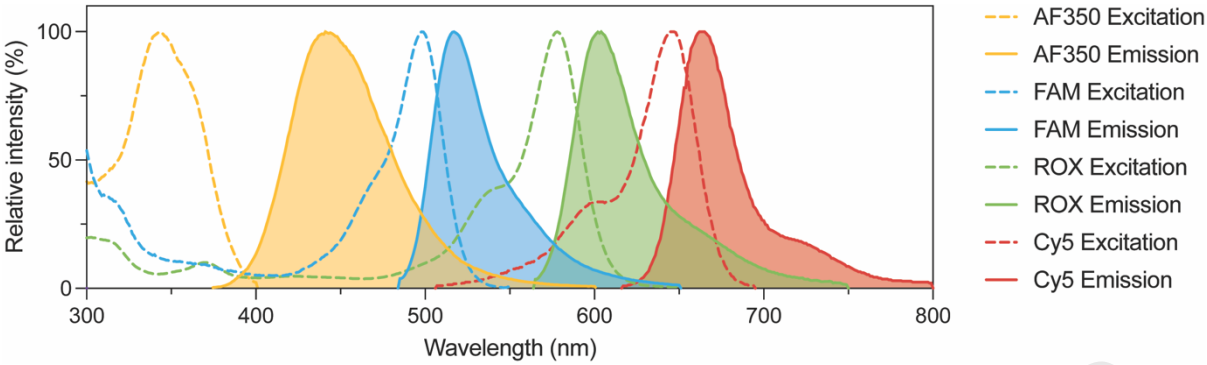

Figure 3. Excitation and emission spectra for AF350, FAM, ROX and Cy5. Data adapted from Fluorescence SpectraViewer (ThermoFisher Scientific).

3WJ:

`Y1-FAM: 5′-FAM-TTT TCA CCG CTC TGG TCC TC-3′`

`Y2-ROX: 5′-ROX-TTT TCA GGC TGT GAG CGG TG-3′`

`Y3-Cy5: 5′-Cy5-TTT TGA GGA CCA ACA GCC TG-3′`

dsDNA:

`Z1-FAM: 5′-FAM-TTT TAA CAC ATG CAG GAC GGC GCT T-3′`

`Z2-Cy5: 5′-Cy5-TTT TAA GCG CCG TCC TGC ATG TGT T-3′`

HJ:

`B-Cy5:  5′-Cy5-TTT TGC CTA GCA TGA TAC TGC TAC CG-3′`

`H-AF350: 5′-AF350-TTT TCG GTA GCA GTA CCG TTG GTG GC-3′`

`R-ROX:  5′-ROX-TTT TGC CAC CAA CGG CGT CAA CTG CC-3′`

`X-FAM:  5′-FAM-TTT TGG CAG TTG ACG TCA TGC TAG GC-3′`

2.3 Gel electrophoresis

Multiplex polyacrylamide gel electrophoresis (PAGE) was performed to evaluate the non-canonical 3WJ and HJ structures that are formed. To correctly visualise both structures, it was necessary to independently optimise the PAGE conditions for the 3WJ and HJ.

2.3.1 Formation of 3WJ

The 3WJ was analysed using 20% native Tris acetate PAGE (50 mM Trizma Acetate—Sigma-Aldrich (Merck), T1258—along with 75 mM NaCl and 5 mM $MgCl_2$, pH 6.1). Each combination of fluorescent 3WJ strands (*i.e.* `Y1, Y2, Y3, Y1-Y2, Y1-Y3, Y1-Y2-Y3`) and control dsDNA (*i.e.* `Z1, Z2, Z1-Z2`) and 3WJ and dsDNA (*i.e.* `Y1-`

Y2-Y3 and Z1-Z2) were mixed in HEPES buffer (10 mM HEPES—Sigma-Aldrich (Merck), H0887—along with 750 mM NaCl, 50 mM $MgCl_2$, pH 7.0) and incubated at 37 ºC for 2 hours, prior to the addition of loading dye (6X, 2.5% Ficoll®-400, 11 mm EDTA, 3.3 mM Tris-HCl, 0.017% SDS, 0.15% Orange G, pH 8—New England Biolabs, B7022S). Each sample was loaded onto the gel, which was then run at 70 V for 240 min, post-staining was not required since all sequences were fluorescently labelled (supplementary Figure S1). Fluorescent sequences were then imaged using a multiplex assay (G:Box 9 mini—Syngene). FAM (ex. blue, em. 525), ROX (ex. Green, em. 605 nm) and Cy5 (ex. Red, em. 705 nm) were captured separately, the images were overlayed, and a false colour applied to distinguish each fluorophore labelled sequence (GeneSys software—Syngene).

2.3.2 Analysis of binding to 3WJ

The ability of ΛΛ-Fe^{II}_2LLD to bind with the 3WJ was analysed by 20% native PAGE. A solution of $(NH_4)_2Fe(SO_4)_2$•$6H_2O$ was mixed with the LLD peptide ligand in a 2:1 ratio to form ΛΛ-Fe^{II}_2LLD, as previously described.[17] 3WJ junction strands (5 pmol) were mixed in HEPES buffer (10 mM HEPES, 750 mM NaCl, 50 mM $MgCl_2$, pH 7.0) and 1-1000 equivalents of pre-complexed ΛΛ-Fe^{II}_2LLD (5-5000 pmol) was added, and incubated at 37 ºC for 2 hours. Loading dye (6X, 2.5% Ficoll®-400, 11 mm EDTA, 3.3 mM Tris-HCl, 0.017% SDS, 0.15% Orange G, pH 8—New England Biolabs, B7022S) was added, and the gel was run and visualised as described above (supplementary Figure S3).

2.3.3 Evaluation of non-canonical HJ structures

The HJ was probed for its ability to generate other higher order pseudo-duplex DNA. Pseudo-duplex structures were analysed using polyacrylamide gel electrophoresis (PAGE) using a 12% native Tris Borate EDTA (TBE) gel composition (1x TBE pH 6.0, adjusted to pH 6 with 6 M acetic acid—FisherScientific, 10031223). Each combination of fluorescent HJ strands (*i.e.* B, H, R, X, B-H, B-R, B-X, H-R, H-X, R-X, B-H-R-X) were mixed in H_2O (nuclease-free) containing 10 mM phosphate, 150 mM NaCl, 2 mM $MgCl_2$, at pH 6.0 at a concentration of 10 pmol, melted and annealed to room temperature prior to the addition of loading dye. Samples required no post-gel staining, and were run for 180 min at 50 V, and imaged using a multiplex assay (G:Box 9 mini—Syngene). AF350 (ex. UV, em. 441 nm), FAM (ex. Blue, em. 525), ROX (ex. Green, em. 605 nm) and Cy5 (ex. Red, em. 705 nm) images were captured separately (supplementary Figure S2), overlayed, and a false colour applied to distinguish each fluorophore labelled sequence (GeneSys software—Syngene).

2.3.4 Band densitometric analysis of HJ DNA formation induced by BA-C6

HJ DNA must be prepared from oligomers that are annealed on the same day as use. A Cy5-labelled sequence and three non-labelled strands (B-Cy5, H, R and X) were used in this study whereby Cy5 enabled HJ visualisation and subsequent quantification without interference from other fluorescent signals. Annealing was performed by heating samples to 95 ºC and cooled in 5 ºC increments to 4 ºC (annelaing was performed on a Mastercycler® nexus—Eppendorf). Samples with HJ DNA (10 pmol) and 0.5-250 equivalents of BA-C6 (2.5-1250 pmol) were mixed in nuclease-free H_2O and incubated at 37 ºC for 1 hour. A single stranded control (Cy5-B

strand, 10 pmol), HJ control (10 pmol in nuclease-free H_2O), and buffered HJ control (10 pmol, 10 mM phosphate, 150 mM NaCl, 2 mM $MgCl_2$, pH 6.0) were prepared to serve as reference for compound-induced HJ formation. DNA loading dye (6X, 10 mM Tris-HCl, 0.03% bromophenol blue, 0.03% xylene cyanole FF, 60% glycerol, 60 mM EDTA—ThermoScientific, R0611) was added and the samples were analysed by 12% native PAGE (1x TBE—FisherScientific, 10031223—adjusted to pH 6.0 with acetic acid). The gel was run at 50 V for 180 min and visualised using red excitation together with a 705 nm filter (G:Box 9 mini—Syngene). Band densitometry was performed in triplicate to evaluate formation of the HJ (GeneTools software—Syngene). All samples were compared to control sequences run without BA-C6 with the relative intensities plotted and analysed in GraphPad Prism (supplementary Figure S5).

2.3.5 Multiplex analysis of HJ formation by BA-C6

Samples were prepared as described above using 0.5-40 equivalents of BA-C6, but with fluorophore labelled HJ sequences (`B-Cy5`, `H-AF350`, `R-ROX`, `X-FAM`—10 pmol). After incubation for 1 h at 37 ºC, loading dye (6X, 10 mM Tris-HCl, 0.03% bromophenol blue, 0.03% xylene cyanole FF, 60% glycerol, 60 mM EDTA—ThermoScientific, R0611) was added and samples were loaded onto 12% native PAGE gel (1x TBE—FisherScientific, 10031223—adjusted to pH 6.0 with 6 M acetic acid). The gel was run at 50 V for 180 min and visualised without staining using a multiplex assay (G:Box 9 mini—Syngene): AF350 (ex. UV, em. 441 nm); FAM (ex. Blue, em. 525); ROX (ex. Green, em. 605 nm); and Cy5 (ex. Red, em. 705 nm) images were captured separately, overlayed (supplementary Figure S4), and a false colour applied to distinguish each fluorophore labelled sequence (GeneSys software—Syngene).

2.4 Microscale Thermophoresis

2.4.1 Experimental design

Microscale thermophoresis experiments were developed using a fluorescently labelled target (3WJ or HJ DNA) and the non-labelled ligands (ΛΛ-Fe^{II}_2LLD or BA-C6). Therefore, 3WJ, HJ, and the dsDNA off-target each contained one Cy5 labelled strand as outlined below.

3WJ:

```
Y1:     5′-CAC CGC TCT GGT CCT C-3′

Y2:     5′-CAG GCT GTG AGC GGT G-3′

Y3-Cy5: 5′-Cy5-TTT TGA GGA CCA ACA GCC TG-3′
```

dsDNA:

```
Z1:     5′-AAC ACA TGC AGG ACG GCG CTT-3′

Z2-Cy5: 5′-Cy5-TTT TAA GCG CCG TCC TGC ATG TGT T-3′
```

HJ:

B-Cy5: 5′-Cy5-TTT TGC CTA GCA TGA TAC TGC TAC CG-3′

H: 5′-CGG TAG CAG TAC CGT TGG TGG C-3′

R: 5′-GCC ACC AAC GGC GTC AAC TGC C-3′

X: 5′-GGC AGT TGA CGT CAT GCT AGG C-3′

2.4.2 Binding of ΛΛ-Fe^{II}_2LLD to 3WJ DNA

MST (Monolith—NanoTemper Technologies GmbH) requires ≥16 samples that have a constant concentration of fluorescently labelled target and a serial dilution of the ligand. Binding affinity experiments were performed using the red LED channel with automatic power (*i.e.* 80%) and the temperature was set at 25 ºC. The Cy5-3WJ target (20 nM) was sufficiently luminescent and a maximum ΛΛ-Fe^{II}_2LLD ligand concentration of 50 μM was employed. ΛΛ-Fe^{II}_2LLD (20 μL, 100 μM) was added to sample 1 and then a serially diluted with 0.1% Tween-80 HEPES buffer (0.1% Tween-80, 10 mM HEPES, 750 mM NaCl, 50 mM $MgCl_2$, pH 7) for samples 2 to 16. Tween was included in the buffer to mitigate the effects of DNA condensation by the cationic ligand. Cy5-3WJ (10 μL, 40 nM) was added to all samples and solutions were mixed but not vortexed. Samples were centrifuged to remove air bubbles and incubated at 37 ºC for 5 min. Each sample was then loaded into a glass capillary (Monolith standard capillary—NanoTemper Technologies GmbH, MO-K022) and placed into the sample tray. It is important not to touch the centre of the capillaries as this can impede accurate analysis. Controls with non-metallated LLD peptide ligand, $(NH_4)_2Fe(SO_4)_2{\bullet}6H_2O$ (Mohr's salt), and Cy5-3WJ alone were also performed, and each assay was repeated in triplicate.

2.4.3 MST with ΛΛ-Fe^{II}_2LLD and dsDNA

Next, the binding affinity for ΛΛ-Fe^{II}_2LLD with dsDNA was investigated. Here, two discrete experiments were performed; i) ΛΛ-Fe^{II}_2LLD with Cy5-dsDNA; and ii) ΛΛ-Fe^{II}_2LLD with Cy5-dsDNA and non-labelled 3WJ.

i) Cy5-dsDNA (20 nM) was incubated with a serial dilution of ΛΛ-Fe^{II}_2LLD (starting at 100 μM) in 0.1% Tween-80 HEPES buffer (0.1% Tween-80, 10 mM HEPES, 750 mM NaCl, 50 mM $MgCl_2$, pH 7.0) at 37 ºC for 5 min. Samples were loaded into glass capillaries (Monolith standard capillary—NanoTemper Technologies GmbH, MO-K022) and MST was performed.

ii) Cy5-dsDNA (20 nM) and non-fluorescently labelled 3WJ (20 nM) were incubated with ΛΛ-Fe^{II}_2LLD, as described above. MST was performed and data was compared to Cy5-3WJ and Cy5-dsDNA.

2.4.4 Data analysis for ΛΛ-Fe^{II}_2LLD and 3WJ

MST data was imported into the MO.Affinity Analysis software (NanoTemper Technologies GmbH) and the dissociation constant (K_d) was calculated. During MST analysis fluorescence inhomogeneity and the presence of aggregates were observed (Figure S6), which is due to DNA condensation, a similar effect which was observed

during PAGE analysis of ΛΛ-Fe^{II}_2LLD and 3WJ DNA (*vide infra* Figure 5). Due to this effect, the K_d was calculated based on the initial fluorescence, rather than at a specific time-point during the MST analysis. This analysis was performed in triplicate on all samples and the data plotted in GraphPad Prism, with standard deviation shown as error bars.

The MO.Affinity Analysis software (NanoTemper Technologies GmbH) uses the K_d fit model to describe a molecular interaction with 1:1 stoichiometry according to the law of mass action.

$$f(c) = Unbound + (Bound - Unbound) \cdot \frac{c + c_t + K_d - \sqrt{(c + c_t + K_d)^2 - 4 \cdot c \cdot c_t}}{2c_t}$$

Where $f(c)$ is the fraction bound at a given concentration c;

Unbound is the F_{norm} signal of the target alone;

Bound is the F_{norm} signal of the complex;

K_d is the dissociation constant (or binding affinity);

c_t is the final concentration of target in the assay.

2.4.5 Binding of BA-C6 to HJ DNA

In a similar manner to the 3WJ assay, BA-C6 (100 μM, 20 μL) was added to sample 1 and then a serial dilution with water was performed for samples 2 to 16. Pre-annealed Cy5-HJ (40 nM, 10 μL) was then added to all samples and solutions were mixed, but not vortexed. Samples were centrifuged to remove air bubbles and incubated at 37 ºC for 60 min. Next, samples loaded into a glass capillary (Monolith standard capillary—NanoTemper Technologies GmbH, MO-K022) and placed into the Monolith sample tray. Care was taken to avoid touching the centre of the capillary. MST binding affinity was performed, as described above, with BA-C6 with HJ, 9-amino-acridine (9-NH_2-acridine; Sigma-Aldrich (Merck)—92817) with HJ and HJ alone. A dsDNA control with BA-C6 was also performed. MST experiments were repeated in triplicate.

2.4.6 Data Analysis for the Holliday Junction

The MST data for BA-C6 with Cy5-HJ was analysed using the MO.Affinity Analysis software (NanoTemper Technologies GmbH), but the Hill model with EC_{50} fit was used to analyse cooperative binding instead of the K_d model used for the 3WJ. The EC_{50} was more applicable in this situation as there is state change in the target whereby the HJ changes from the open-X to the stacked-X form upon binding of the BA-C6 ligand.

$$f(c) = Unbound + \frac{(Bound - Unbound)}{1 + \left(\frac{EC_{50}}{C}\right)^{n_{Hill}}}$$

Where $f(c)$ is the fraction bound at a given concentration c;

Unbound is the F_{norm} signal of the target alone;

Bound is the F_{norm} signal of the complex;

EC_{50} is half of the maximal concentration;

n_{Hill} is the Hill coefficient and describes the cooperativity of the reaction.

3. Results and Discussion

3.1 Polyacrylamide gel electrophoresis

3.1.1 Multiplex fluorescent PAGE

Fluorophore labelled sequences (section 2.2) were designed to facilitate evaluation of 3WJ or HJ binding ligands. The 3WJ sequences were labelled with FAM, ROX and Cy5, while AF350 was also included for the HJ. Each strand of the 3WJ, the sequences that form pseudo duplexes, and the combined 3WJ strands and a control dsDNA were incubated at 37 ºC for 2 hours prior to PAGE separation. The gel was then visualised using a multiplex assay that enabled the emission of each strand to be imaged independently (Figure 4a). The colour applied to each fluorophore enables the visualisation of each sequence, and the subsequent overlay of images indicates the presence of two or more strands where blue (FAM) and red (Cy5) produce purple hybridised strands, and green (ROX) and red (Cy5) produce orange pseudo-duplexes. The 3WJ can be visualised as pinkish-yellow colour from hybridisation of blue (FAM), green (ROX), and red (Cy5).

This assay was also applicable for the analysis of the non-canonical structures formed by the HJ strands. Here, the four sequences (`B`, `H`, `R` and `X`, shown in red, yellow, green, and blue, respectively) were analysed and their ability to form pseudo-duplexes. As expected, not all strands form duplexes (Figure 4b) due to their complementarity. For example, `B-R` and `H-X` do not form pseudo-duplexes as they are not designed to bind within the HJ. On the contrary `B-H`, `B-X`, `H-R` and `X-R`, which have complementarity, can form pseudo-duplexes, and can be visualised by the overlaid colours—orange (`B-H`), pink (`B-X`), light green (`H-R`) and turquoise (`X-R`)—in these samples (Figure 4b). Finally, when the four HJ sequences (`B`, `H`, `R` and `X`) were incubated together we observed a light-yellow band for formation of the 4-way HJ, which is an overlay of the four fluorescent signals (Figure 4b).

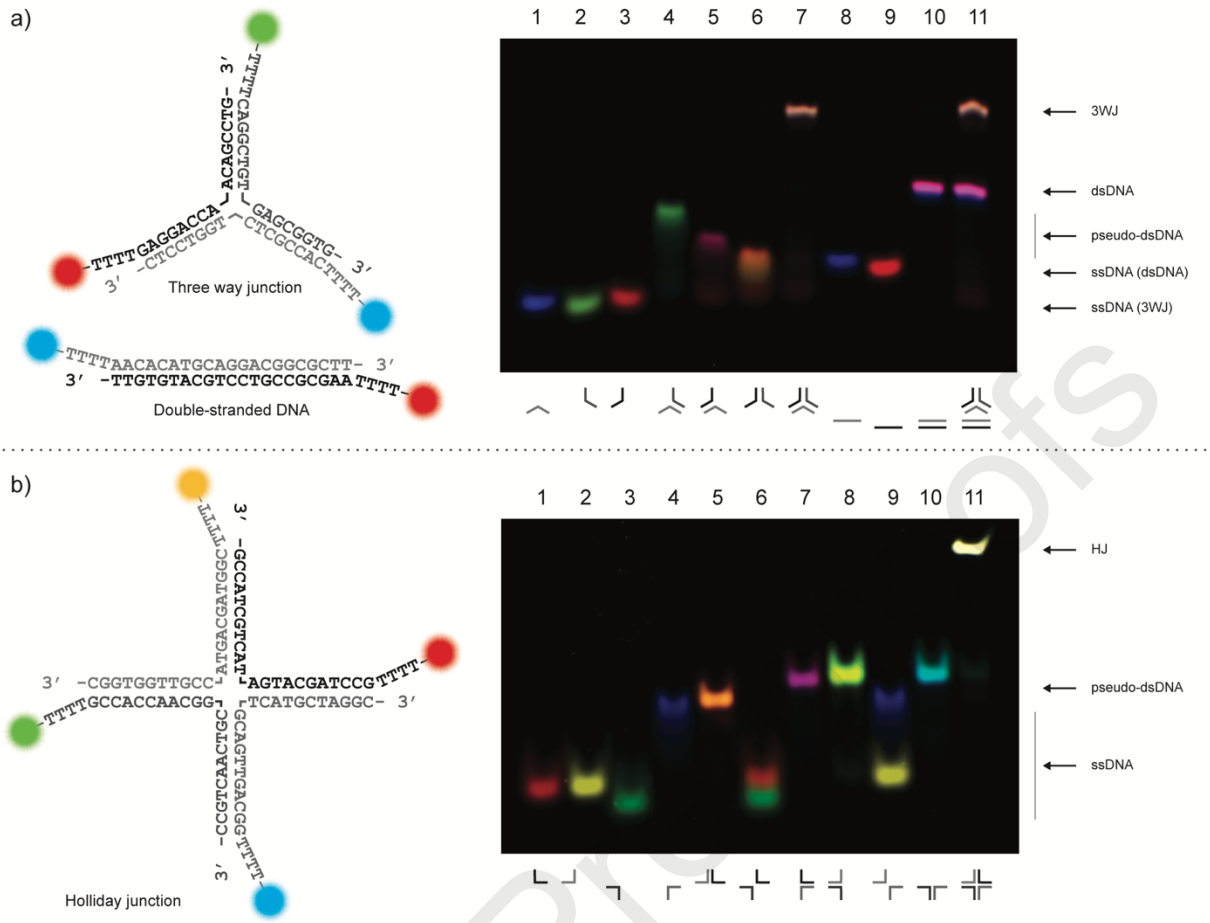

Figure 4. Multiplex assay for native PAGE analysis of 3WJ and HJ sequences. a) Lanes 1-3: `Y1`, `Y2` and `Y3`, respectively; Lane 4: `Y1-Y2`; Lane 5: `Y1-Y3`; Lane 6: `Y2-Y3`; Lane 7: 3WJ (`Y1-Y2-Y3`); Lane 8-9: `Z1` and `Z2`; Lane 10: dsDNA (`Z1-Z2`); Lane 11: 3WJ (`Y1-Y2-Y3`) and dsDNA (`Z1-Z2`). FAM (`Y1`), ROX (`Y2`) and Cy5 (`Y3`) labelled sequences were independently visualised (see supplementary Figure S1) and the images overlayed. b) Lanes 1-4: `B`, `H`, `R` and `X`, respectively; Lane 5: `B-H`; Lane 6: `B-R`; Lane 7: `B-X`; Lane 8: `H-R`; Lane 9: `H-X`; Lane 10: `R-X`; Lane 11: HJ (`B-H-R-X`). AF350 (`H`), FAM (`X`), ROX (`R`) and Cy5 (`B`) filters were employed for visualisation of each sequence (Figure S2) and the structures they form.

3.1.2 DNA binding studies

Next, the DNA binding profile of a peptide helicate and a bis-acridine derivative with 3WJ and HJ DNA, respectively, was analysed by native PAGE. The ΛΛ-Fe^{II}_2LLD helicate was previously studied by Gómez-González *et al*. (2021) and 3WJ-binding was reported.[17,18] Similarly, the binding of BA-C6[29] with HJ DNA was reported by the Cardin[26] and Searcey[27] groups, who performed X-ray crystallography and PAGE analysis to evaluate the interactions of BA-C6 with the HJ.

The ability of ΛΛ-Fe^{II}_2LLD to bind with the labelled 3WJ was assessed. Here, 3WJ DNA was incubated with ΛΛ-Fe^{II}_2LLD (1-1000 equivalents) at 37 ºC for 2 hours and the samples were analysed by PAGE (Figure 5a). The 3WJ forms in the presence of ΛΛ-Fe^{II}_2LLD and is observed as a pinkish-yellow band—arising from an overlay of FAM (blue), ROX (green) and Cy5 (red) fluorescent signals. At higher ΛΛ-Fe^{II}_2LLD concentrations, the intensity of the 3WJ decreases in a manner consistent with condensation of the 3WJ.

BA-C6 was previously shown to bind with and induce HJ DNA formation[26, 27] and here this analysis is expanded to multiplex gel electrophoresis with samples prepared in water rather than buffer—for clear visualisation of the HJ. The fluorophore labelled HJ strands (`B-Cy5`, `H-AF350`, `R-ROX` and `X-FAM`) were incubated in water (without salt or buffer) and with increasing concentrations of BA-C6, HJ formation and then condensation was observed. The HJ can be observed across all samples but the intensity of the band increases with additional BA-C6, and, at 20 equivalents an upward shift for the HJ is observed (Figure 5b). This signifies binding of BA-C6 and a change in HJ conformation. A change in the pseudo-duplex band is also observed as the DNA adopts the junction conformation. In the presence of higher concentrations of BA-C6 we observed DNA condensation, which is not surprising as multiple bis-acridine molecules have bound with HJ DNA and formed aggregates. Finally, band densitometry was performed with the Cy5-labelled HJ to determine the relative concentration of HJ present in each sample (supplementary Figure S5). An increase in HJ was observed, reaching its maximum at 30 equivalents of BA-C6, followed by a stepwise decrease in HJ DNA from 40-250 equivalents, which appears due to DNA condensation.

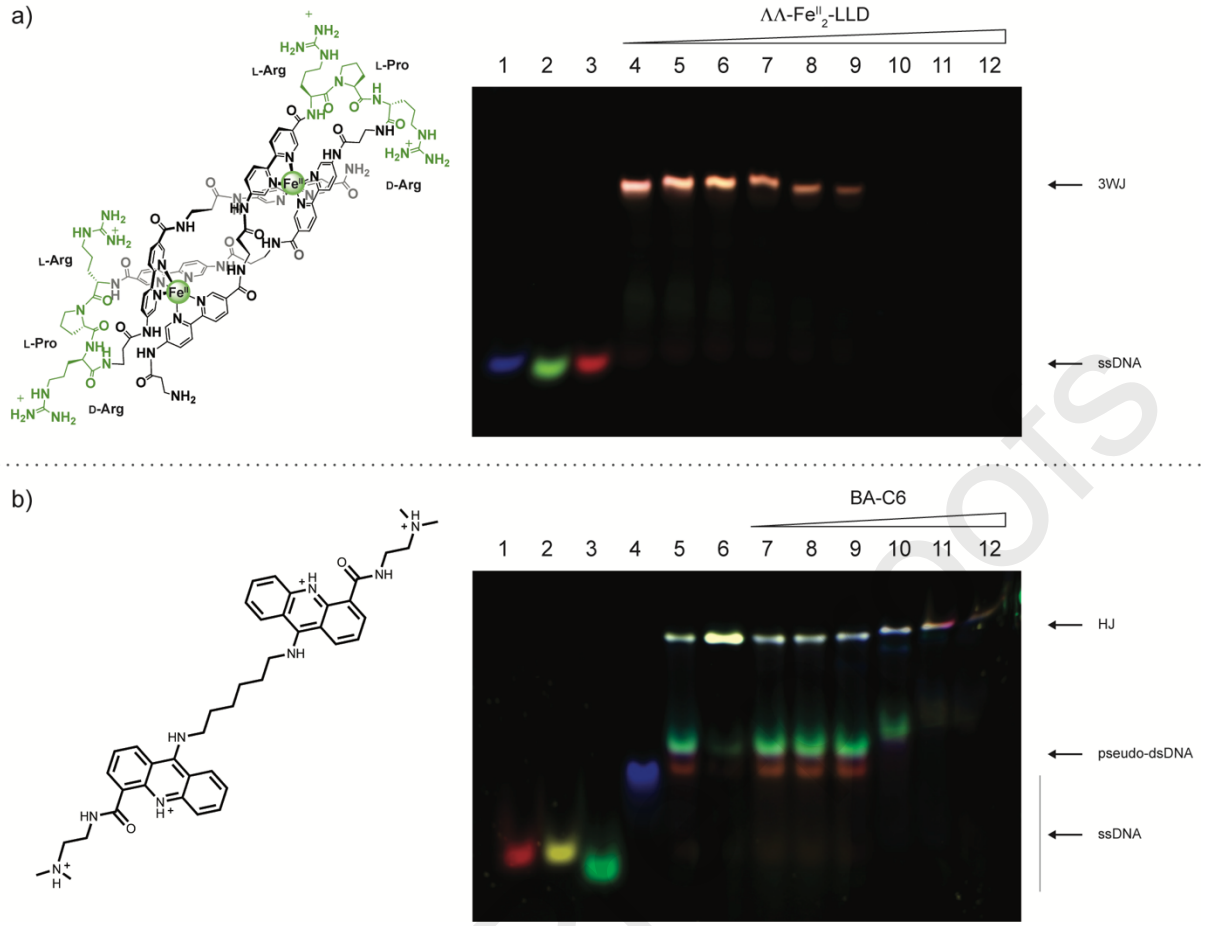

Figure 5. Native PAGE analysis of the binding of ΛΛ-Fe$^{II}_2$LLD and BA-C with 3WJ and HJ DNA, respectively. a) Lane 1: `Y1`; Lane 2: `Y2`; Lane 3: `Y3`; Lanes 4-12: 3WJ (`Y1-Y2-Y3`) with 1-1000 equivalents of ΛΛ-Fe$^{II}_2$LLD. DNA condensation is observed after 25 eq. Fe^{II} helicate with complete condensation at 100 eq. Individual images can be found in Figure S3. b) Lane 1: `B`; Lane 2: `H`; Lane 3: `R`; Lane 4: `X`; Lane 5: Negative control of HJ (`B`, `H`, `R` and `X`) in H_2O; Lane 6: Positive control of HJ (`B`, `H`, `R` and `X`) incubated in phosphate buffer (10 mM phosphate, 150 mM NaCl, 2 mM $MgCl_2$); Lanes 7-12: HJ (`B`, `H`, `R` and `X`) with 0.5-40 equivalents of BA-C6. HJ formation and condensation were observed in the presence of the bis-acridine derivative, with almost complete condensation in the presence of 40 eq. BA-C6. The control experiments were performed as a comparison for the profile of ssDNA (`B`, `H`, `R` and `X`), pseudo-duplexes (control 1), open-X HJ DNA, and the unbound stacked-X HJ in the presence of salts (control 2).

3.2 Microscale thermophoresis

Thermophoresis describes the movement of a molecule through a temperature gradient, and this movement is dependent on the size, charge, and hydration shell of the molecule.[32] The thermophoretic mobility of the molecule will therefore also change upon interaction with a ligand, and this forms the basis of microscale thermophoresis (MST).[32-37] MST is performed in thin glass capillaries and requires one partner in the interaction (*i.e.* ligand or target molecule) to be fluorescent,[37] which in this study is the junction DNA. Cy5-labelled 3WJ (Figure 6) and HJ DNA (Figure 7) were designed, with Cy5 attached to a short poly-thymine linker.

3.2.1 Binding constant of ΛΛ-Fe$^{II}_2$LLD with 3WJ DNA

To evaluate the binding affinity of ΛΛ-Fe$^{II}_2$LLD with the 3WJ, a serial dilution of the Fe^{II} helicate—starting at the highest concentration at 50 μM—was performed in MST buffer

(0.1% Tween-80 HEPES buffer, pH 7). Cy5-3WJ (20 nM) was added and the samples were incubated at 37 ºC for 5 min. Samples were then loaded into glass capillaries and MST was performed. Aggregates were observed at higher concentrations of ΛΛ-Fe^{II}_2LLD, an effect which was also observed during the gel electrophoresis experiments (Figure 5a). However, DNA condensation impacts MST analysis as it reduces the fluorescent signal, so methods to limit aggregate formation were tested. Buffers at different pH, concentration ranges, and incubation times were investigated, and it was found that 0.1% Tween-80 within HEPES buffer was the most suitable. While condensation of the 3WJ DNA was still evident, it was reduced to a level compatible with MST. Since aggregates were present, the fluorescent signal was not uniform across the tested sample range (supplementary Figure S6), and the MST traces could not be used to determine the dissociation constant (K_d). Consequently, the K_d was calculated from a change in initial fluorescence (Figure 6). This change in initial fluorescence of Cy5-3WJ DNA treated with ΛΛ-Fe^{II}_2LLD was plotted and the K_d value was calculated as 3.033 x10^{-8} M. Controls of LLD peptide ligand, an Fe^{II} salt, and 3WJ alone were also evaluated but no significant binding was detected.

Next, the binding of ΛΛ-Fe^{II}_2LLD with Cy5-dsDNA was investigated. Here, two different experiments were performed: i) ΛΛ-Fe^{II}_2LLD and Cy5-dsDNA; and ii) ΛΛ-Fe^{II}_2LLD and Cy5-dsDNA in the presence of 3WJ. In the second experiment the 3WJ was not fluorescently labelled and therefore binding to the 3WJ would not be detected (or would be silent) by MST and determined indirectly by changes in the Cy5-dsDNA sequence present. Samples were prepared as previously described and the K_d was evaluated using initial fluorescence. Binding was observed for ΛΛ-Fe^{II}_2LLD with Cy5-dsDNA (K_d = 3.743 x 10^{-9} M) in the absence of 3WJ junction. However, when Cy5-dsDNA and the non-fluorescent 3WJ were both incubated with ΛΛ-Fe^{II}_2LLD, no binding of Cy5-dsDNA was detected (Figure 6). This shows that although the Fe^{II}-helicate can bind with both 3WJ and dsDNA, the helicate preferentially binds with 3WJ DNA, indicating that ΛΛ-Fe^{II}_2LLD is a selective binder of replication *foci* in cells. This result is therefore in excellent agreement with earlier reports.[17,18]

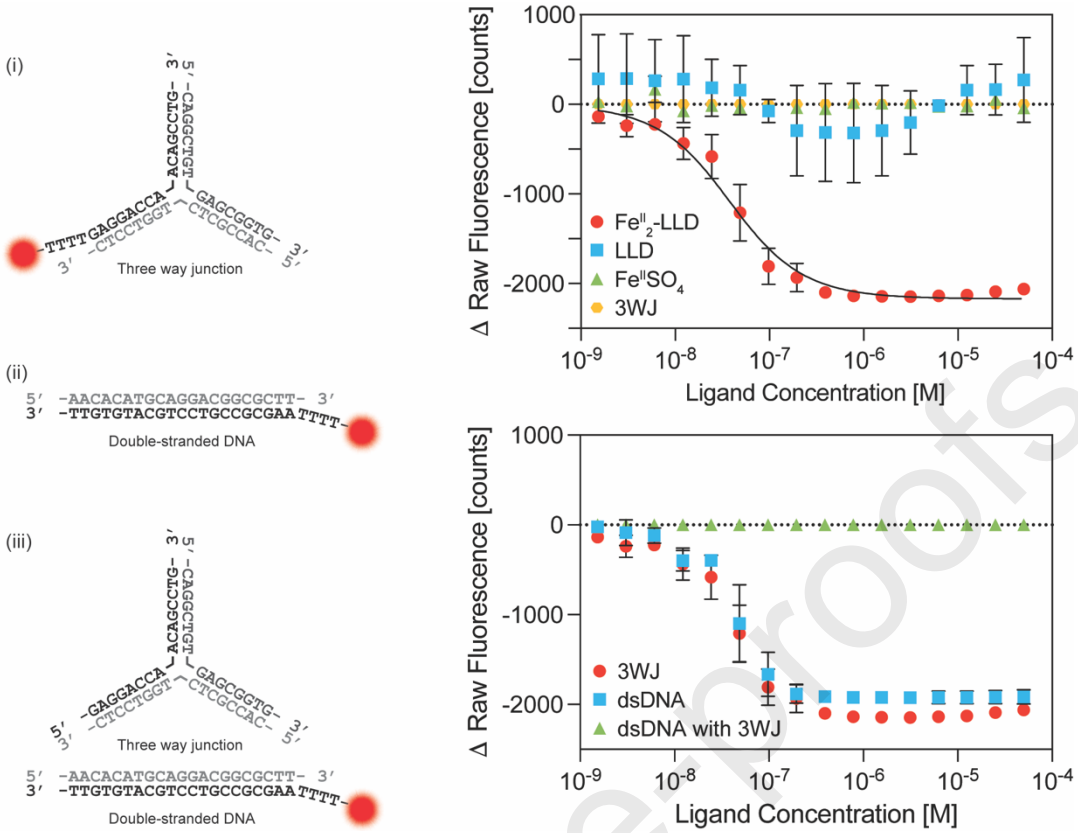

Figure 6. Binding affinity of ΛΛ-Fe$^{II}_2$LLD with Cy5-3WJ and Cy5-dsDNA. Top: The change in initial fluorescence of Cy5-3WJ across a serial dilution of ΛΛ-Fe$^{II}_2$LLD was plotted (red circle) and the K_d determined. Controls with LLD (blue square), Fe^{II}SO$_4$ (green triangle) and 3WJ-alone (yellow hexagon) were also plotted. Upon binding of ΛΛ-Fe$^{II}_2$LLD with Cy5-3WJ a decrease in fluorescence was observed, no significant change in raw fluorescence was detected for LLD or Fe^{II}SO$_4$, which indicates that no binding has occurred with the Cy5-3WJ. Bottom: Change in initial fluorescence of Cy5-3WJ (i), Cy5-dsDNA (ii) and Cy5-dsDNA with non-labelled 3WJ (iii) in the presence of ΛΛ-Fe$^{II}_2$LLD. The Fe-helicate binds with Cy5-3WJ (red circle) and Cy5-dsDNA (blue square) with similar affinities (change in initial fluorescence), but ΛΛ-Fe$^{II}_2$LLD does not bind with Cy5-dsDNA in the presence of 3WJ (green triangle). This demonstrates that ΛΛ-Fe$^{II}_2$LLD can bind both 3WJ and dsDNA, but that is preferentially binds with the 3WJ.

3.2.2 Interaction of BA-C6 with HJ DNA

MST was also employed to evaluate the interaction of BA-C6 with HJ DNA. A serial dilution from 50 µM BA-C6 was performed, Cy5-HJ DNA (20 nM) was added, and the samples were incubated at 37 ºC for 1 hour. MST was performed, but in a similar manner to the Fe^{II} helicate, BA-C6 induced DNA condensation at higher concentrations. Mitigation efforts to reduce DNA condensation were investigated including, lower drug-DNA incubation times, detergents and systems comprising methyl cellulose, but these had little impact on the DNA condensation effects observed. Consequently, the change in initial fluorescent intensity was also employed to investigate the binding of BA-C6 with the HJ (Figure 7). Control experiments including a mono-acridine type ligand, 9-amino-acridine, and dsDNA were also performed and compared to BA-C6 with HJ DNA. Here, the change in normalised fluorescent signal were plotted and fit to the Hill model for ligand-target interactions (Figure 7). EC_{50} values of 4.359 x10^{-7} M and 2.406 x10^{-7} M were obtained for the interaction of BA-C6 with Cy5-HJ DNA and a Cy5-dsDNA control, respectively, which shows that BA-C6 binds HJ and dsDNA with similar affinity. Previous studies of BA-C6 with HJ[26-28] and dsDNA[29] indicate that the compound can also bind dsDNA, with

many acridine derivatives displaying similar properties. Furthermore, in this work a 9-amino-acridine monomer was screened for its HJ-binding interaction, but at the same concentration range it failed to fully bind to the HJ and the data was subsequently unable to fit using the Hill model (Figure 6).

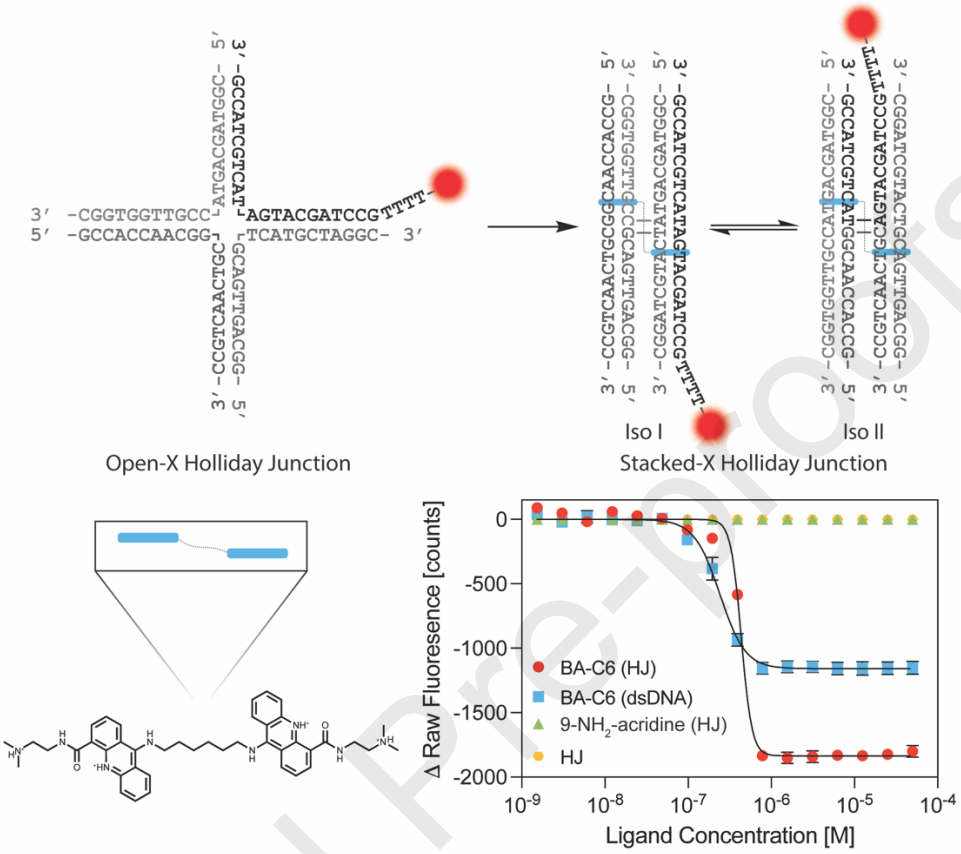

Figure 7. MST analysis of BA-C6 and controls with Cy5-HJ DNA. Open-X HJ is incubated with BA-C6 and upon binding it induces the formation of stacked-X HJ (Iso I or Iso II can form). BA-C6 induces changes in initial fluorescence when incubated with Cy5-HJ (red circle) and Cy5-dsDNA (blue square), but 9-NH_2-acridine (green triangle) is not capable of binding with Cy5-HJ under the same concentration range and the profile observed is comparable to HJ alone (yellow hexagon).

4. Conclusion

A multiplex fluorescent PAGE assay was combined with microscale thermophoresis to elucidate the recognition of 3WJ and HJ DNA binding agents. ΛΛ-Fe^{II}_2LLD and BA-C6 were selected for this study as earlier work[17, 18, 26-28] identified their 3WJ and HJ DNA recognition. Here, we reported the design and application of a multiplex PAGE assay that enables the independent visualisation of each strand of junction DNA. This multiplex assay significantly expands the resolution of previous fluorophore-labelled PAGE experiments enabling the elucidation of both the junction formation and critical intermediates. MST is a relatively new technique and consequently a limited number of DNA binding ligands have been evaluated.[35-40] To our knowledge, these results are the first examples of MST being used to probe the binding affinity of 3WJ- and HJ-binding agents. The adaptation of the MST conditions to overcome ligand-induced fluorescent changes will enable the application of MST for a wider range of ligand-target interactions. In summary, the multiplex PAGE and MST assays reported here demonstrate the selectivity of ΛΛ-Fe^{II}_2LLD and BA-C6 for binding with junction DNA

and can aid the discovery and design of future therapeutics targeting non-canonical nucleic acid structures.

Acknowledgements

None.

Formatting of funding sources

Funding: This work was supported by the Irish Research Council [grant numbers EPSPD/2022/164, GOIPG/2020/472 and IRCLA/2022/3815]; we acknowledge funding from the European Union's Horizon 2020 research and innovation program under the Marie Sklodowska-Curie grant agreement No 861381 [NATURE-ETN]; this project has received funding from Science Foundation Ireland [12/RC/2275_P2]. M.V.L. acknowledges PID2021-127857NB-I00 by MCIN/AEI/10.13039/ 501100011033 and by ERDF A way of making Europe, Fundación Científica de la Asociación Española Contra el Cáncer (Ideas Semilla 2021 – IDEAS211154VÁZQ) and Xunta de Galicia (ED431C 2021/29).

References

1. J. Watson*, et al.*, *Nature*, 1953, **171**, 737-738.

2. R. Franklin*, et al.*, *Nature*, 1953, **171**, 740-741.

3. M. Wilkins*, et al.*, *Nature*, 1953, **171**, 738-740.

4. C. J. Leonard*, et al.*, *Prog. Nucleic Acid Res. Mol. Biol.*, 1994, **48**, 29-52.

5. R. Holliday, *Genet. Res.*, 1964, **5**, 282-304.

6. M. Gellert*, et al.*, *PNAS*, 1962, **48**, 2013-2018.

7. K. Gehring*, et al.*, *Nature*, 1993, **363**, 561-565.

8. A. M. Zahler*, et al.*, *Nature*, 1991, **350**, 718-720.

9. Z. Yu*, et al.*, *Angew Chem. Int. Ed.*, 2015, **127**, 1921-1925.

10. A. Zaid*, et al.*, *ChemBioChem*, 2004, **5**, 1550-1557.

11. I. Gamba*, et al.*, *Chem. Commun.*, 2014, **50**, 11097-11100.

12. J. Malina*, et al.*, *Chemistry - Eur. J. Chem.*, 2007, **13**, 3871-3877.

13. M. R. Singleton*, et al.*, *Cell*, 2001, **107**, 79-89.

14. M. Ortiz-Lombardía*, et al.*, *Nat. Struct. Biol.*, 1999, **6**, 913-917.

15. B. F. Eichman*, et al.*, *PNAS*, 2000, **97**, 3971-3976.

16. A. Oleksi*, et al.*, *Angew. Chem. Int. Ed.*, 2006, **45**, 1227-1231.

17. J. Gómez-González*, et al.*, *Angew. Chem. In.t Ed.*, 2021, **60**, 8859-8866.

18. J. Gómez-González*, et al.*, *Front Chem.* 2018, **6**:520.

19. S. A. Barros*, et al.*, *Angew. Chem. Int. Ed.*, 2014, **53**, 13746-13750.

20. Y. Takezawa*, et al.*, *Dalton Trans.*, 2023, DOI: 10.1039/d3dt01508d.

21. W. Wang*, et al.*, *Sci, Rep.*, 2016, **6**, 22863.

22. K. Ghosh*, et al.*, *JBC*, 2005, **280**, 8290-8299.

23. B. F. Eichman*, et al.*, *J. Mol. Biol.*, 2001, **308**, 15-26.

24. Q. Yin*, et al.*, *Biochem. Pharmacol.*, 2021, **193**, 114767.

25. J. S. Craig*, et al.*, *JACS*, 2023, DOI: 10.1021/jacs.3c00118.

26. A. L. Brogden*, et al.*, *Angew. Chem. Int. Ed.*, 2007, **46**, 3850-3854.

27. L. A. Howell*, et al.*, *ChemMedChem*, 2012, **7**, 792-804.

28. L. A. Howell*, et al.*, *Chem. Comm.*, 2011, **47**, 8262.

29. L. P. G. Wakelin*, et al.*, *J. Med. Chem.*, 2003, **46**, 5790-5802.

30. W. A. Denny*, et al.*, *J. Med. Chem.*, 1985, **28**, 1568-1574.

31. D. R. Duckett*, et al.*, *Cell Press*, 1988, **55**.

32. S. Duhr*, et al.*, *PNAS*, 2006, **103**, 19678-19682.

33. S. Duhr*, et al.*, *EPJE*, 2004, **15**, 277-286.

34. P. Baaske*, et al.*, *Angew Chem. Int. Ed.*, 2010, **49**, 2238-2241.

35. M. Jerabek-Willemsen*, et al.*, *Assay Drug Dev Technol.*, 2011, **9**, 342-353.

36. S. A. Seidel*, et al.*, *Methods*, 2013, **59**, 301-315.

37. C. Entzian*, et al.*, *Methods*, 2016, **97**, 27-34.

38. M. Jerabek-Willemsen*, et al.*, *J. Mol. Struct.*, 2014, **1077**, 101-113.

39. M. G. Costales*, et al.*, *Cell Chem. Biol.*, 2019, **26**, 1180-1186 e1185.

40. D. Jacob*, et al.*, *Angew Chem. Int. Ed.*, 2019, **58**, 9565-9569.